

# A twelve-analyzer detector system for high-resolution powder diffraction

Peter L. Lee,\* Deming Shu,\* Mohan Ramanathan, Curt Preissner, Jun Wang, Mark A. Beno, Robert B. Von Dreele, Lynn Ribaud, Charles Kurtz, Sytle M. Antao, Xuesong Jiao and Brian H. Toby

Advanced Photon Source, Argonne National Laboratory, Argonne, IL 60439, USA.

E-mail: pllee@aps.anl.gov, shu@aps.anl.gov

A dedicated high-resolution high-throughput X-ray powder diffraction beamline has been constructed at the Advanced Photon Source (APS). In order to achieve the goals of both high resolution and high throughput in a powder instrument, a multi-analyzer detector system is required. The design and performance of the 12-analyzer detector system installed on the powder diffractometer at the 11-BM beamline of APS are presented.

© 2008 International Union of Crystallography  
Printed in Singapore – all rights reserved

**Keywords:** multi-analyzer; instrumentation; powder diffraction.

## 1. Introduction

There are many important materials that do not form single crystals. Single crystals are often unavailable for new materials during the period following their initial discovery, when interest is greatest. For such materials, powder diffraction is often the only tool for obtaining detailed structural information. Furthermore, as the use of powder diffraction for crystal structure determination continues to improve and be applied to ever larger structures (*e.g.* Margiolaki *et al.*, 2007), there will be an increased demand for instrumentation with the highest resolution. Easy access to a powder diffraction instrument that can produce a high-quality high-resolution powder pattern in a timely fashion has become very important for many research programs.

In an earlier publication, Hastings *et al.* (1984) demonstrated using perfect-crystal-optics parallel-beam geometry to obtain high-resolution powder diffraction data. The information from a high-resolution powder pattern enhances the ability for both structure determination and phase identification. However, the major drawback of this high-resolution measurement is that it is very time-consuming. Using a single-point detector with a perfect-crystal analyzer discards almost all the photons diffracted by the powder sample during the measurement. With a typical synchrotron source, recording a simple pattern with a  $2\theta$  step of  $0.001^\circ$  and a 1 s counting time covering  $90^\circ$  would require more than 24 h. This inefficiency has limited the availability of this powder technique. In order to reduce the measuring time, multi-analyzer systems have been developed at several synchrotron facilities (Toraya *et al.*, 1996; Hodeau *et al.*, 1998; Siddons *et al.*, 1998; D'Amico *et al.*, 2003). The recent use of two-dimensional detectors such as image plates or CCDs and linear detectors such as the newly developed microstrip detectors has achieved fast data collec-

tion with reasonably good resolution in the measurement of powder data with well collimated intense synchrotron X-ray beams (Nishibori *et al.*, 2001; Schmitt *et al.*, 2003; Siddons *et al.*, 2007; Sarin *et al.*, 2008). However, compared with the two-dimensional detectors or linear detectors that are normally able to obtain powder data with  $\sim 10^{-3}$  angular resolution, analyzer crystal detector systems that can provide  $\sim 10^{-4}$  angular resolution are better suited to resolving peak overlap. Furthermore, the analyzer, which also functions as an angular slit and provides energy discrimination, can minimize unwanted signals such as fluorescence and scatter from ancillary equipment. The high-resolution capability is advantageous for complex structural analyses such as proteins and phase transition studies with small structural changes, while the low background is ideal for resonant scattering measurements. Several synchrotron facilities have selected between these two different approaches for their dedicated powder instruments, such as the multi-analyzer system at the European Synchrotron Radiation Facility (Fitch, 1996) and the curved image-plate system at SPring-8 (Nishibori *et al.*, 2001). These two kinds of system are complementary and have advantages for different types of measurements. The materials science beamline at the Swiss Light Source has adopted a hybrid design for powder diffraction that offers both in a single instrument, using a microstrip detector to achieve rapid data measurement and a multi-analyzer crystal detector system to achieve high resolution (Patterson *et al.*, 2005). The new beamline at the Diamond Light Source is also planned to do the same (Tartoni *et al.*, 2008). We have developed an instrument at the Advanced Photon Source (APS) 11-BM beamline with an advanced multi-analyzer system that is dedicated to high-resolution measurements. To improve on existing multi-analyzer systems, the design we present here offers full individual angular control on the analyzer crystals

that allows fully optimized peak shapes and intensity, thus achieving high resolution with high throughput.

## 2. Instrumentation

### 2.1. Mechanical design requirements

The optical layout for 11-BM, a bending-magnet beamline, consists of a vertical beam collimation mirror, a double-crystal monochromator with a horizontal sagittal-focusing second crystal, and a vertical focusing mirror that can be tuned over the range 4.8–40 keV. Details of the beamline will be published elsewhere (Wang *et al.*, 2008). The multi-analyzer system was designed to cover the same energy range as the beamline. The most effective use of the instrument dictates that the data must be merged into a single composite pattern. This requires that the peak widths and peak shape be almost identical for all detectors or else the merging process will degrade the instrument performance, limiting options for measurements and thus degrading the data quality. In addition, the  $2\theta$  angular coverage of the multi-analyzer system should be kept reasonably large, while the angular increment between the neighboring analyzers are kept reasonably small. This requires a design in which the analyzers must fit into a narrow angular space. Based on these requirements, the following specifications were defined:

- (i) Analyzer  $\theta$  angular range will cover the energy range 4.8–40 keV using Si(111) or Ge(220) analyzer crystals with sub-millidegree precision.
- (ii) Reasonable range of analyzer  $\chi$  angle adjustment to avoid asymmetric peak shape owing to  $\chi$  misalignment.
- (iii) Detectors individually mounted on analyzer  $2\theta$  arms.
- (iv) Two degrees of angular separation between neighbouring analyzers.
- (v) 12 analyzers for the system.
- (vi) A slit box located between the sample and the analyzers to reduce background scattering.
- (vii) Collimation to prevent detection of scattering other than directly from the sample.

### 2.2. Multi-analyzer detector system

As shown in Fig. 1, the 12-analyzer detector system (1) is mounted on the main circle of a high-resolution two-circle diffractometer (2) comprised of customized 480 and 420 goniometers from Huber GmbH, Germany. With a three-dimensional adjustable supporting table (3), the diffractometer has dimensions of 2600 mm (h)  $\times$  2100 mm (l)  $\times$  1700 mm (w). A detailed description of the diffractometer and its associated robotic sample handling system will be published elsewhere (Wang *et al.*, 2008).

The 12-analyzer detector system achieves a  $2^\circ$  separation between neighboring analyzers with all 12 analyzers fitting into the space limited by the radius of the main goniometer. To overcome this technical challenge, the 12 analyzers and detectors are grouped into two types of subassemblies: six left-side units and six right-side units. The resulting interleaved analyzer crystal assemblies are mounted on both sides of the

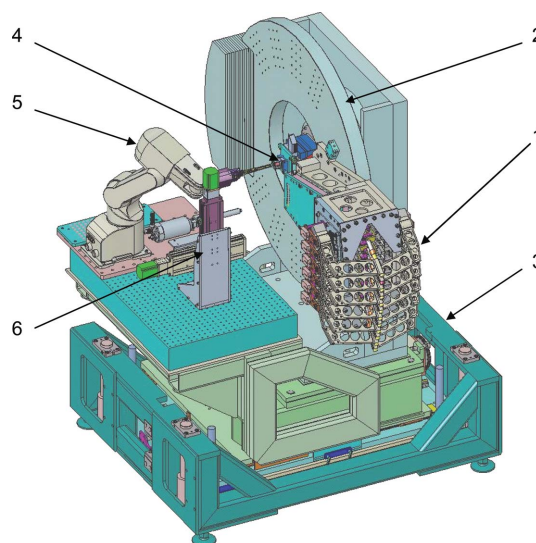


**Figure 1**

A three-dimensional model of the high-resolution diffractometer with 12-analyzer detector system: (1) 12-analyzer detector system, (2) two-circle goniometer, (3) supporting table, (4) sample stages, (5) sample mounting robot, (6) stages for cryostream.

vertical plane defined by the incoming X-ray beam direction and center of the sample.

For each of the analyzer crystals there are three positioning devices to control the crystal orientations with coarse and fine  $\theta$  angle motion and independent  $\chi$  angle adjustment. The  $\theta$  angle coarse motion is provided by an Aerotech ART50 rotary stage, which has a 12.6 arcsec unidirectional positioning repeatability and a 3.6 arcsec home positioning repeatability. The  $\theta$  angle fine motion is a compact PZT-driven sine bar type using an overconstrained rotary weak-link mechanism developed at APS (Shu *et al.*, 2001, 2003; Shu, Toellner *et al.*, 2007). This provides an ultimate positioning resolution better than 0.05 arcsec with 0.5 arcsec repeatability (Shu, Lee *et al.*, 2007). The overconstrained rotary weak-link mechanism provides much higher structural stiffness and stability than traditional kinematic linear spring flexure mechanisms. A Picomotor-driven tilt stage for the analyzer crystal  $\chi$  angle adjustment is positioned on the center of the planar rotary shaft through an adapter plate. Fig. 2(a) shows a three-dimensional model of the individual analyzer and Fig. 2(b) shows a photograph of an analyzer pair for mounting on opposite sides of the analyzer subassembly.

Fig. 3 shows front and side views of a three-dimensional model of the 12-analyzer detector system. To reduce background scattering, a slit box with 12 pairs of slits is mounted on the base frame (1) of the detector system in front of the analyzer subassembly (2). The slit box consists of an aluminium frame (3), tantalum blades to prevent cross-talk (4), and 24 slit inserts (5). The tantalum knife-edge slit inserts are precisely exchangeable to cover the slit size range from 0.2 mm to 3 mm for various applications. If needed, the slit box can be sealed with Kapton film and purged with helium gas for low-energy X-ray experiments. Since detectors require a less precise  $2\theta$ -positioning specification, cost-effective rotary

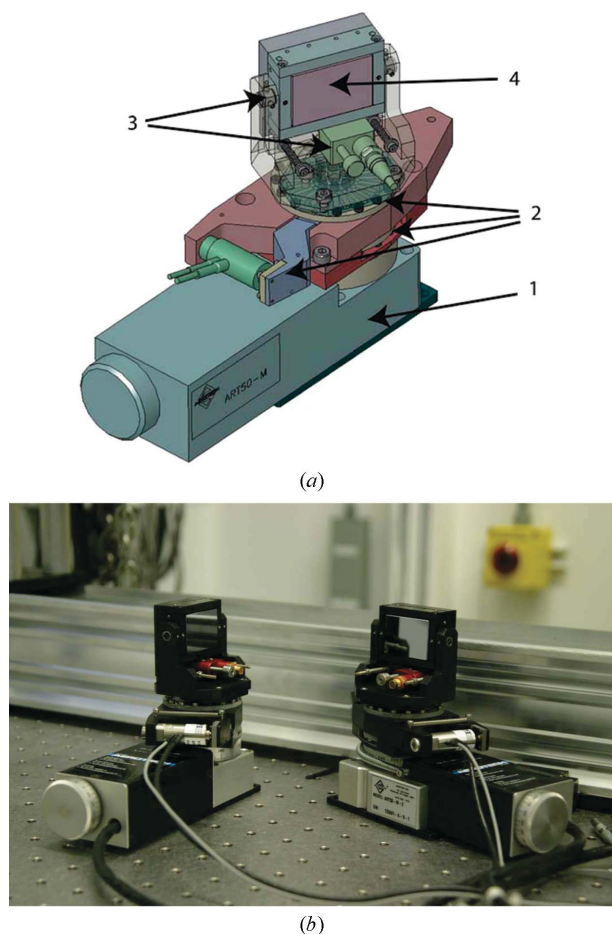


**Figure 2**  
 (a) Three-dimensional model of an individual analyzer: (1) Aerotech ART50 rotary stage providing  $\theta$  angle coarse motion, (2) PZT-driven sine bar using an overconstrained rotary weak-link mechanism providing  $\theta$  angle fine motion, (3) Picomotor-driven tilt stage for  $\chi$  motion, (4) analyzer crystal and its housing. (b) Photograph of right- and left-hand analyzer subassemblies.

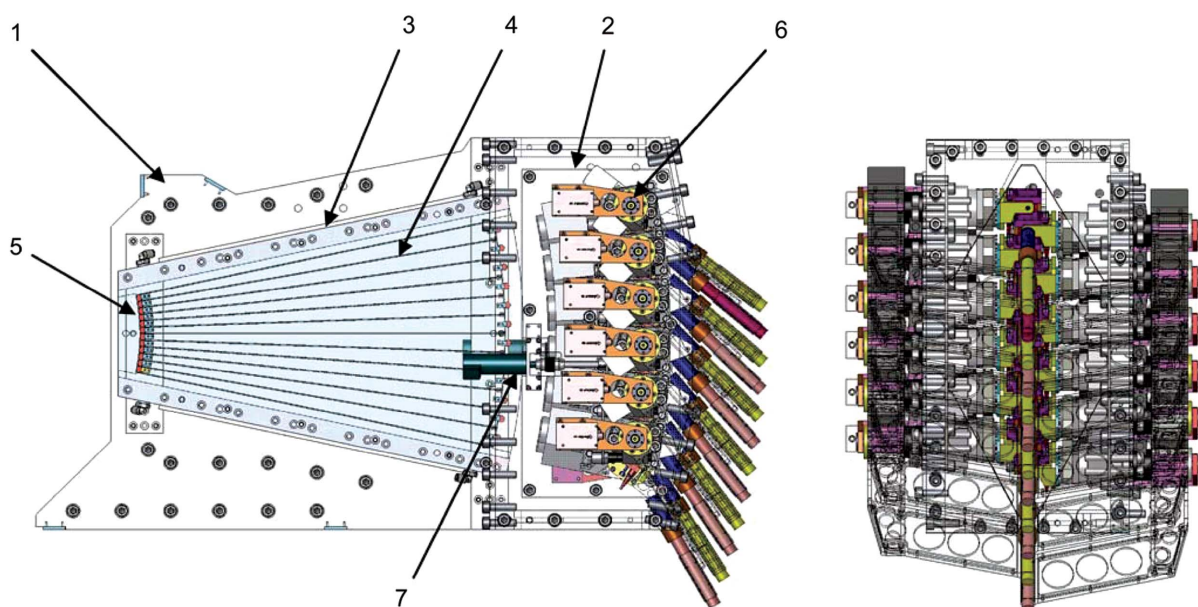


**Figure 3**  
 Front and side views of a three-dimensional model of the 12-analyzer detector system: (1) base frame, (2) analyzers subassembly, (3) slits box frame, (4) tantalum isolating blades, (5) slit insert, (6) rotary stage for detector, (7) stepper motor with gear-reducer.

stages (6) were chosen for this angular motion control. Each side of the analyzer/detector subassembly, composed of six units, is driven by one stepping motor (7) coupled to the stages through a gear-reducer and a timing-belt chain.

### 3. Experimental set-up

The multi-analyzer detector diffractometer was installed in the experimental station at the 11-BM beamline (Lee *et al.*, 2004; Wang *et al.*, 2008) at APS. A monochromatic beam, focused to about the location of the analyzers at 30.862 keV ( $0.401738 \text{ \AA}$ ), was used for initial alignment of the diffractometer and analyzers. Twelve Si(111) crystals were used as analyzers and 12 LaCl<sub>3</sub> scintillation detectors (Cyberstar from Oxford-Danfysik) were employed to record the diffraction patterns. The X-ray beam was aligned to be parallel to the rotating surface of the two-circle diffractometer and pass through the two-circle diffractometer center of rotation, the slit box and then the analyzers. This alignment was performed by moving the diffractometer  $2\theta$  angle to  $0^\circ$  and then to  $180^\circ$  to locate the slit box upstream and downstream of the diffractometer and taking exposures at the outer side of the slit box position with a piece of photosensitive paper. The diffractometer table was rotated about the vertical axis, according to the difference in the positions of the two burn marks until repeated measurements showed burn marks in line with each other and at the same distance from the diffractometer surface. Then, an alignment pin was placed at the center of rotation of the diffractometer. By adjusting the  $xy$  translation of the diffractometer table we aligned the X-ray beam to be through the center of rotation and the slit box. The analyzers were mounted downstream of the slit box and kinematically aligned. A NIST SRM 640c silicon powder sample was loaded in a 0.7 mm Kapton capillary, attached to a Hampton Research magnetic base, and then mounted on a DC

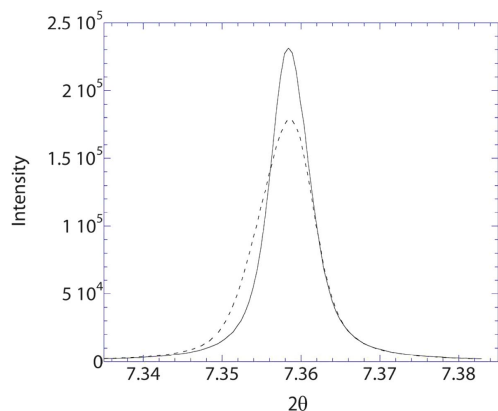


**Figure 4** Si(111) diffraction peak from one of the analyzers before (dash) and after (solid) adjustment of  $\chi$ .

motor spinner centered on the goniometer  $2\Theta$  axis. The spinner has a top speed of about 15000 rpm adjustable by a 0–10 V DC voltage input.

Initially, all 12 analyzer  $\theta$  and  $2\theta$  positions were moved to their theoretical angles. The analyzers were then adjusted to the correct  $\theta$  angle using the direct X-ray beam. A PIN diode detector was used for this initial tuning before installation of the Cyberstar scintillation detectors for powder diffraction measurements. Then the analyzer  $\chi$  angles were adjusted using the Si(111) powder diffraction peak. By adjusting the analyzer  $\chi$  angle in this way, we are able to optimize the intensity and the peak shape of the powder diffraction peak obtained from each individual analyzer. Optimizing the analyzer  $\chi$  angles has proven to be the crucial adjustment required to obtain the best diffraction peak shape from each individual analyzer (Fig. 4) and thus obtain consistency among all the analyzers and allow them to be summed without loss of resolution. Fig. 5 shows the individual Si(111) diffraction peaks from 12 analyzers, and the FWHM of these diffraction peaks are listed in Table 1. It is important to point out that the analyzer  $\chi$  adjustments must be done with a powder diffraction peak and not the direct beam to obtain the optimal diffraction peak shape.

#### 4. Data measurements and analysis

The diffractometer is controlled by Experimental Physics and Industrial Control System (EPICS) (Kraimer, 1998) using a Motif Editor and Display Manager (MEDM) based user interface (Evans, 2006). Using the  $2\theta$  motor pulses as the channel advance input for the multi-channel scaler (Struck SIS3820), the continuous scan mode was employed for data acquisition to eliminate the motor positioning overhead time in step scan mode. A standard sample consisting of 33 wt% of NIST Si standard (SRM 640c) and 67 wt% of NIST  $\text{Al}_2\text{O}_3$  standard (SRM 676) was prepared for calibration measurements. For initial commissioning, a full measurement at 30.862 keV (0.401738 Å) of the mixed Si/ $\text{Al}_2\text{O}_3$  standard was used to calibrate each powder pattern from the 12 individual analyzers. The powder pattern was recorded in  $0.0005^\circ$   $2\theta$

**Table 1**

Full width at half-maximum (FWHM) of the Si(111) reflection from a Si/ $\text{Al}_2\text{O}_3$  standard mixture for each of the 12 individual analyzers.

Analyzer No.	FWHM	Analyzer No.	FWHM
1	0.00599 (5)	7	0.00614 (5)
2	0.00600 (5)	8	0.00590 (5)
3	0.00592 (5)	9	0.00585 (5)
4	0.00619 (5)	10	0.00611 (5)
5	0.00603 (5)	11	0.00604 (5)
6	0.00617 (5)	12	0.00603 (4)

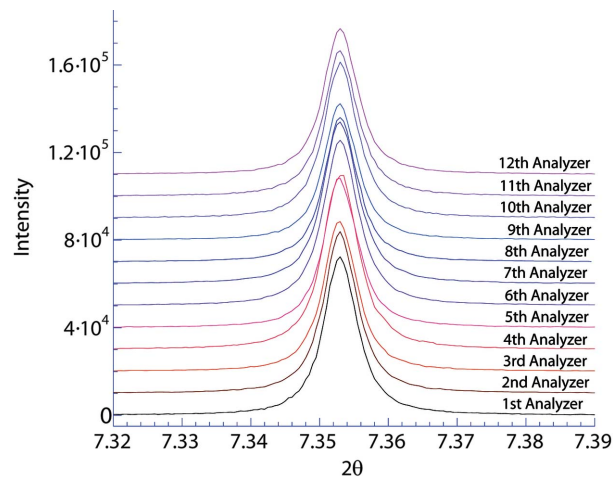


**Figure 5** Si(111) diffraction peaks of mixed Si/ $\text{Al}_2\text{O}_3$  standard from 12 individual analyzers. The intensity is scaled to counts  $\text{s}^{-1}$  (100 mA) $^{-1}$  of ring current individually without correction for detector sensitivity. The intensities are also offset by 10000 between the neighboring analyzers for clarity.

intervals with a  $2\theta$  angle scanning speed of  $3.333^\circ \text{ min}^{-1}$ , thus covering  $50^\circ$   $2\theta$  in 2.77 h and yielding 100000 steps. The 12 individual powder diffraction patterns were analyzed using the Rietveld method (Rietveld, 1967) using the program GSAS (Larson & Von Dreele, 2004) with the EXPGUI user interface (Toby, 2001). The certified cell parameter ( $a = 4.54311946 \text{ \AA}$ ) of the NIST Si standard defines the X-ray wavelength. We were able to refine the structure of the mixed Si/ $\text{Al}_2\text{O}_3$  standard sample and fit instrumental constants independently for each of the 12 powder patterns. The resulting zero offsets, wavelengths and scale factors are shown in Table 2. Applying corrections for each of these three parameters allows the 12 diffractograms to be merged into a single pattern using linear interpolation. After correcting for the slight deviations from the nominal  $2^\circ$  spacing between detectors and the minor wavelength differences, intensities on a regularly spaced grid are obtained as shown in Fig. 6. Powder patterns can be merged using these same parameters regardless of differences in scan range and scan speed for different data measurements. However, it is necessary to recalibrate if the energy is changed or after realignment of the diffractometer owing to a change in the source position. The program *CMPR* (Toby, 2005), a utility program for powder diffraction, has been updated to include options for reading the powder pattern in the 11-BM data format, retrieving the calibration results from the refinements

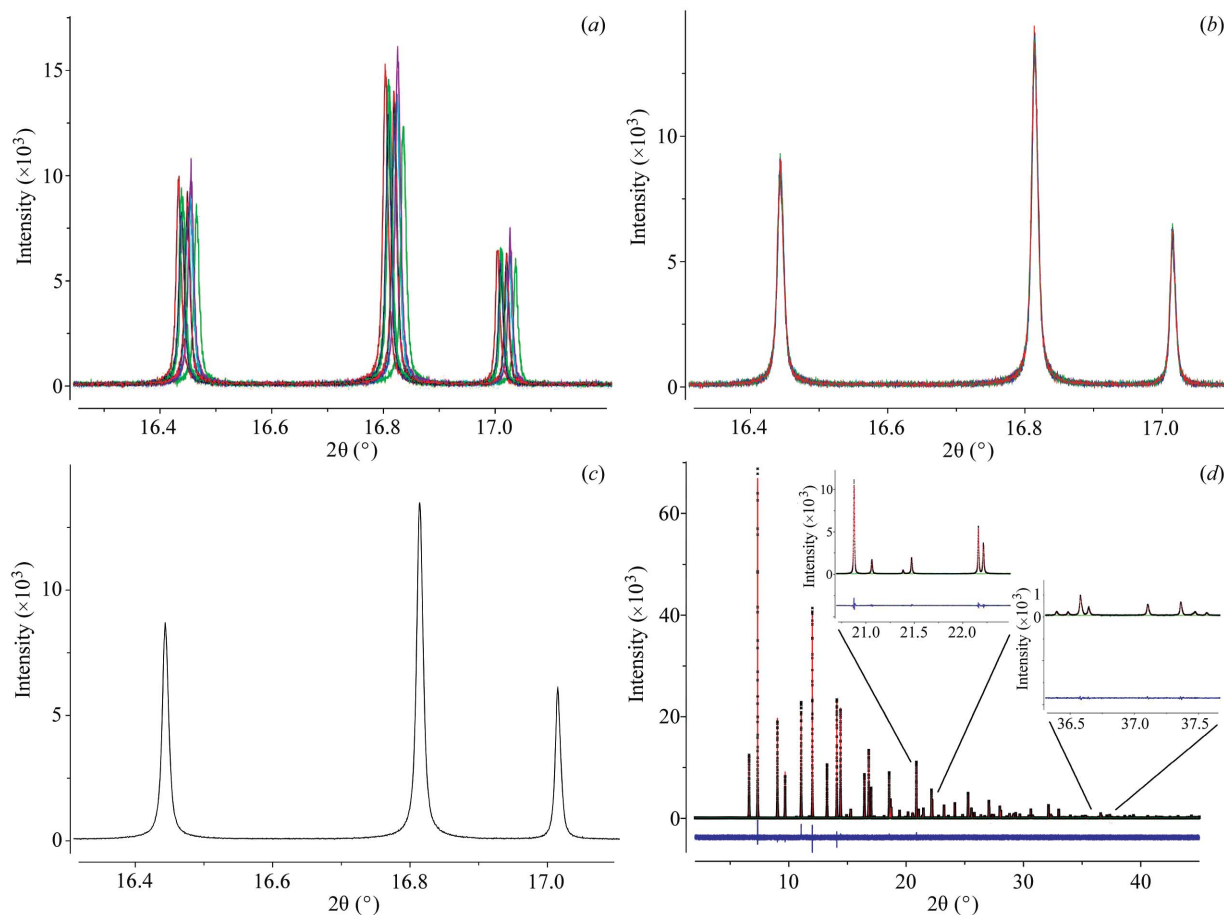


**Figure 6**

A section of a powder pattern of  $\text{Si}/\text{Al}_2\text{O}_3$  measured at 30.862 keV (0.401738 Å) displays the data-merging process: (a) a section of the raw data showing each of the 12 analyzers with only monitor correction and scaled to 100 mA synchrotron ring current; (b) the previous 12 diffractograms, but now corrected with the sensitivity, zero and wavelength calibration results listed in Table 2; (c) the merged diffractogram; (d) fitting of the merged pattern, with data marked as crosses, a solid red line for the calculated pattern, and the blue curve under the pattern for differences. Residuals for the fit are  $R_{\text{wp}} = 9.92\%$ ,  $R_p = 7.2\%$  and  $\chi^2 = 2.204$ .

**Table 2**

Calibration parameters for analyzers.

These are based on the data extracted from structural refinement of data from a  $\text{Si}/\text{Al}_2\text{O}_3$  standard with separate fits for each analyzer. The relative efficiency was determined from the refinement.

Analyzer No.	$2\theta$ zero offset	Relative efficiency	Wavelength (Å)
1	9.99102 (1)	0.9855 (19)	0.4016626 (4)
2	7.997986 (1)	0.9726 (19)	0.4016367 (4)
3	6.00215 (2)	1.0495 (18)	0.4016700 (4)
4	3.98417 (1)	0.8396 (20)	0.4016405 (4)
5	1.99088 (2)	1.0371 (18)	0.4016714 (4)
6	0.00684 (2)	0.9026 (19)	0.4016511 (4)
7	-1.99789 (2)	0.9215 (19)	0.4016671 (4)
8	-4.01037 (2)	1.1000 (18)	0.4016413 (5)
9	-6.00923 (2)	1.1477 (18)	0.4016601 (5)
10	-8.01565 (2)	1.0000 (19)	0.4016245 (4)
11	-10.00855 (2)	1.0561 (18)	0.4016605 (5)
12	-12.02656 (2)	1.0767 (18)	0.4016269 (5)

of the standard, and merging the data with the appropriate corrections.

The effectiveness of this instrument can be seen in a crystallographic study of  $\text{SrCO}_3$  performed using 11-BM data collected with these settings. The result of the fitting is shown

in Fig. 7 with  $R_{\text{wp}} = 7.2\%$ ,  $R_p = 5.5\%$  and  $\chi^2 = 1.529$ . Following the initial experiments at 30.862 keV, we have measured data at three other energies, 10.101 keV, 20.378 keV and 39.363 keV. It is relatively easy to adjust the analyzers by simply moving their  $\theta$  and  $2\theta$  angles to those for the new energy and then optimizing the analyzer  $\theta$  by scanning the PZT weak-link stage with either the direct beam or a powder diffraction peak from a standard sample. Energy changes do not require adjustment of the analyzer  $\chi$  angle. Fits to merged data from the  $\text{Si}/\text{Al}_2\text{O}_3$  standard mixture at those X-ray energies are included in the supplementary materials.<sup>1</sup>

## 5. Discussion

High-resolution powder diffraction plays an important role in materials research from identifying phases to solving the crystal structure from powder diffraction patterns. The technique is widely used, particularly as synchrotron radiation

<sup>1</sup> Supplementary data for this paper are available from the IUCr electronic archives (Reference: IE5021). Services for accessing these data are described at the back of the journal.

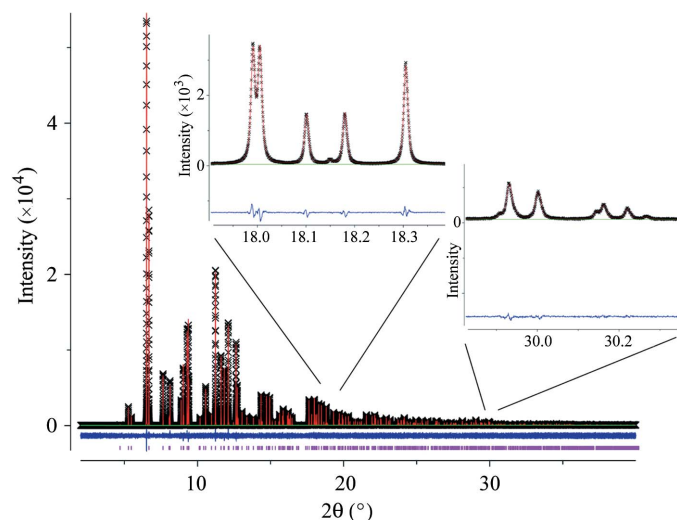


**Figure 7**  
Structure refinement of a SrCO<sub>3</sub> sample [space group *Pm**cn* and lattice parameters 5.107501 (2) Å, 8.413820 (4) Å and 6.026924 (3) Å] using GSAS. The data points are marked with crosses, the reflection positions are marked with vertical red lines, and the calculated pattern and differences are shown with solid red lines. Residuals for the fit are  $R_{wp} = 7.2\%$ ,  $R_p = 5.5\%$  and  $\chi^2 = 1.529$ .

facilities have become more accessible. However, the long data collection time for the conventional single analyzer point detector powder diffractometer has discouraged many researchers. When multi-channel detector systems were introduced about a decade ago (Toraya *et al.*, 1996; Hodeau *et al.*, 1998; Siddons *et al.*, 1998) they allowed data with high resolution and quality to be rapidly collected. Our new design is intended to further improve the data quality and facilitate easy energy changes. By employing independent analyzer stages that can move over a large angular range with excellent accuracy, we are able to change X-ray energies without altering the center location of the X-ray footprint on the analyzer crystals. This ensures the performance consistency of an individual analyzer at large energy ranges. The addition of the  $\chi$  angle adjustment for each crystal analyzer improves the peak shape consistency for the diffraction patterns from all the analyzers, independent of energy. This better preserves the resolution and therefore improves the quality of the merged data. In addition, the 12 detectors at 2° angle increments improve the data collection efficiency. This effect is greater at higher energy (30–40 keV), where a quick 2° scan provides enough angle coverage for rapid collection of a full powder pattern. Consequently, we are able to obtain high-quality high-resolution powder diffraction data more efficiently, making the facility more accessible to researchers with a wide range of scientific interests.

The authors would like to thank Rogelio Ranay for assembling the analyzer system and Dr A. N. Fitch for his advice. The instrument construction project was supported by the US Department of Energy, Office of Science, Office of

Basic Energy Sciences, as part of DOE-BES LAB-03 instrument construction program. Used of the Advanced Photon Source was supported by the US Department of Energy, Office of Science, Office of Basic Energy Sciences, under contract No. DE-AC02-06CH11357.

## References

D'Amico, K., Wasserman, S. & Harlow, R. (2003). Private communication.

Evans, K. (2006). *MEDM Reference Manual*, <http://www.aps.anl.gov/epics/EpicsDocumentation/ExtensionsManuals/MEDM/MEDM.html>.

Fitch, A. N. (1996). *Mater. Sci. Forum*, **228–231**, 219–222.

Hastings, J. B., Thomlinson, W. & Cox, D. E. (1984). *J. Appl. Cryst.* **17**, 85–95.

Hodeau, J. L., Bordet, P., Anne, M., Prat, A., Fitch, A. N., Dooryee, E., Vaughan, G. & Freund, A. (1998). *Proc. SPIE*, **3448**, 353–361.

Kraimer, M. R. (1998). *EPICS Input/Output Controller (IOC) Application Developer's Guide*, <http://www.aps.anl.gov/epics/>.

Larson, A. C. & Von Dreele, R. B. (2004). *General Structure Analysis System (GSAS)*. LANL Report No. LAUR 86–748. Los Alamos National Laboratory, NM, USA.

Lee, P. L., Beno, M. A., Shu, D., Ramanathan, M., Mitchell, J. F., Jorgensen, J. D. & Von Dreele, R. B. (2004). *AIP Conf. Proc.* **705**, 388–391.

Margiolaki, I., Wright, J. P., Wilmanns, M., Fitch, A. N. & Pinotsis, N. (2007). *J. Am. Chem. Soc.* **129**, 11865–11871.

Nishibori, E., Takata, M., Kato, K., Sakata, M., Kubota, Y., Aoyagi, S., Kuroiwa, Y., Yamakata, M. & Ikeda, N. (2001). *Nucl. Instrum. Methods Phys. Res. A*, **467–468**, 1045–1048.

Patterson, B. D., Brönnimann, C., Maden, D., Gozzo, F., Groso, A., Schmitt, B., Stampanoni, M. & Willmott, P. R. (2005). *Nucl. Instrum. Methods Phys. Res. B*, **238**, 224–228.

Rietveld, H. M. (1967). *Acta Cryst.* **22**, 151–152.

Sarin, P., Haggerty, R. P., Yoon, W., Knapp, M., Berghauer, A., Zschack, P., Karapetrova, E., Yang, N. & Kriven, W. M. (2008). In preparation.

Schmitt, B., Brönnimann, C., Eikenberry, E. F., Gozzo, F., Hörmann, C., Horisberger, R. & Patterson, B. (2003). *Nucl. Instrum. Methods Phys. Res. A*, **501**, 267–272.

Shu, D., Lee, P. L., Preissner, C., Ramanathan, M., Beno, M., Von Dreele, R. B., Wang, J., Ranay, R., Ribaud, L., Kurtz, C., Jiao, X., Kline, D., Jemian, P. & Toby, B. (2007). *Proc. SPIE*, **6665**, ON1–8.

Shu, D., Toellner, T. S., Alp, E. E. (2001). *Nucl. Instrum. Methods Phys. Res. A*, **467–468**, 771–774.

Shu, D., Toellner, T. S. & Alp, E. E. (2003). US Patent 6 607 840.

Shu, D., Toellner, T. S., Alp, E. E., Maser, J., Ilavsky, J., Shastri, S. D., Lee, P. L., Narayanan, S. & Long, G. G. (2007). *AIP Conf. Proc.* **879**, 1073–1076.

Siddons, D. P., Hulbert, S. L. & Stephens, P. W. (2007). *AIP Conf. Proc.* **879**, 1767–1770.

Siddons, D. P., Yin, Z., Furenlid, L., Pietraski, P., Li, Z. & Harlow, R. (1998). *Proc. SPIE*, **3448**, 120–131.

Tartoni, N., Thompson, S. P., Tang, C. C., Willis, B. L., Derbyshire, G. E., Wright, A. G., Jaye, S. C., Homer, J. M., Pizzey, J. D. & Bell, A. M. T. (2008). *J. Synchrotron Rad.* **15**, 43–49.

Toby, B. H. (2001). *J. Appl. Cryst.* **34**, 210–213.

Toby, B. H. (2005). *J. Appl. Cryst.* **38**, 1040–1041.

Toraya, H., Hibino, H. & Ohsumi, K. (1996). *J. Synchrotron Rad.* **3**, 75–83.

Wang, J. *et al.* (2008). In preparation.